P8.10   SEASONAL SURFACE SPECTRAL EMISSIVITY DERIVED FROM TERRA MODIS DATA

Yan Chen, Sunny Sun-Mack
Science Applications International Corporation, Hampton, VA 23666

*Patrick Minnis, David F. Young, William L. Smith, Jr.
Atmospheric Sciences, NASA Langley Research Center, Hampton, VA 23681

1.   INTRODUCTION

Surface emissivity is essential for many remote-sensing applications including the derivation of surface skin temperature from satellite-based infrared measurements, the determination of cloud detection thresholds, and the estimation of the surface longwave radiation emission, an important component of the energy budget of the surface-atmosphere interface. Brightness temperature differences, BTD, between 3.7 and 11.0-μm observations are often indicative of the presence or absence of clouds. For clear scenes, the BTD is due to differences in atmospheric absorption and in surface emissivity ε between the two channels. Cloud phase, optical depth, and particle size further affect the BTD in cloudy scenes. Retrieval of cloud phase and effective particle size often relies on the value of BTD, which for optically thin clouds is affected by the surface emission and, at 3.7μm, the surface reflectance. Thus, the accuracy of cloud detection and particle size retrievals depends on the accuracy of the surface emissivity. The CERES (Clouds and the Earth's Radiant Energy System; see Wielicki et al., 1998) Project is measuring broadband shortwave and longwave radiances and deriving cloud properties form various images to produce a combined global radiation and cloud property data set. In this paper, simultaneous data from *Terra* MODIS (Moderate Resolution Imaging Spectroradiometer) taken at 3.7, 8.5, 11.0, and 12.0 μm are used to derive the skin temperature and the surface emissivities at the same wavelengths. The methodology uses separate measurements of clear sky temperature in each channel determined by scene classification during the daytime and at night. The relationships between the various channels at night are used during the day when solar reflectance affects the 3.7-μm radiances. A set of simultaneous equations is then solved to derive the emissivities. Global monthly emissivity maps are derived from *Terra* MODIS data while numerical weather analyses provide soundings for correcting the observed radiances for atmospheric absorption. These maps are used by CERES and other cloud retrieval algorithms.

Corresponding author address: P. Minnis, MS 420 NASA Langley Res. Ctr., Hampton, VA 23681;
email: p.minnis@larc.nasa.gov

2.   DATA

Terra MODIS data taken during July and October 2002 and January and April 2003 were analyzed with the CERES cloud processing algorithms (e.g., Minnis et al. 2003). Each MODIS pixel is classified as either clear or cloudy using the latest update of the CERES method to obtain the clear-sky top-of-the-atmosphere (TOA) brightness temperatures T_i at 3.7, 10.8, 12.0, and 8.5 μm, denoted channels $i = 3$, 4, 5, and 6, respectively. MODIS data have a nominal resolution of 1 km but are sampled at every 2 km for CERES. It is assumed that the scene classification by the method mentioned above is correct for all pixels and, therefore, the temperatures are uncontaminated by clouds. However, that is not always the case and some filtering is required. European Center Medium Range Weather Forecast (ECMWF) analyses provided every 6 hours at a resolution of 1° latitude and longitude were used to specify vertical profiles of atmospheric temperature, humidity, and ozone as well as initial values of surface skin temperature. Linear interpolation was used to match the soundings to the satellite observation times. Standard atmospheric values were used for profiles of other absorbing gases such as NO_2 and CH_4.

3.   METHODOLOGY

The basic approach solves a set of simultaneous equations to obtain surface emissivity. The method uses observations from both daytime and nighttime over the same area.

The relationship between the TOA and surface radiances can be approximated as

$$B_i(T_i) = \varepsilon_{ai}B_i(T_{ai}) + (1-\varepsilon_{ai})B_i(T_{si}) \qquad (1)$$

where B is the Planck function, ε_a and T_a are the effective atmospheric emissivity and effective atmospheric temperature, respectively. The radiance for T_{si}, the apparent skin radiating temperature, is determined using the correlated *k*-distribution method (Kratz 1995) with the atmospheric profiles to remove the molecular absorption. The *k*-distribution technique is used to compute the upwelling radiation at each ECMWF layer over the entire band pass of the channel using the appropriate filter function for the particular satellite imager channel. In the absence of solar radiation, the radiation balance at

surface is

$$B_i(T_{si}) = \varepsilon_i B_i(T_{skin}) \qquad (2)$$

where T_{skin} is the skin temperature and T_{si} is the effective radiating temperature of the surface. For simplicity, it assumed that ε_i does not depend on the viewing zenith angle, VZA. At night, the skin temperature can be expressed as

$$T_{skin} = B_i^{-1}[B_i(T_{si}) / \varepsilon_i] \qquad (3)$$

where B_i^{-1} is the inverse Planck function. If the skin temperature is known, the emissivity can be solved for the remaining channels, e.g.,

$$\varepsilon_3 = [B_3(T_{s3})] / [B_3(T_{skin})] \qquad (4)$$

Both T_{s3} and T_{s4} can be derived at night using (2) and the emissivity ratio,

$$\varepsilon_3' = \varepsilon_3 / \varepsilon_4 = [B_3(T_{s3})] / [B_3(T_{s4})] \qquad (5)$$

can then be computed. If it is assumed that this ratio is a constant for a given surface, then the value of ε_3 can be determined from data taken during the daytime. During the daytime, the apparent channel-3 surface temperature is

$$B_3(T_{s3}) = \varepsilon_3[B_3(T_{skin})] + \alpha_3 \chi S_3' \qquad (6)$$

where χ is the anisotropic correction factor, α_3 is the surface albedo, and S_3', the solar radiation at the surface, is computed from the Earth-sun distance and solar-zenith-angle corrected solar constant attenuated by atmospheric absorption using the k-distribution method. Using Kirchoff's law,

$$\alpha_3 = (1 - \varepsilon_3). \qquad (7)$$

Using (4), (5), and (7) to substitute for the emitted component and for the albedo on the right hand side of (6) and rearranging gives

$$\varepsilon_3 = 1 - \{B_3(T_{s3}) - \varepsilon_3'[B_3(T_{s4})]\}/\chi S_3' \qquad (8)$$

Thus, (8) can be used to estimate ε_3. The absorption coefficients used for the thermal component are applied to the observed 3.7-μm radiance to obtain $B_3(T_{s3})$. Although the atmospheric attenuation of the upwelling solar and emitted 3.7-μm radiances is slightly different for each component, the differences should have a negligible impact on the result. Knowing ε_3, T_{skin} can easily be solved from (6). Then, ε_4, ε_5 and ε_6 are computed from (3).

This technique was tested theoretically using 3 different surface types with ε_3 ranging from 0.73 to 0.97 and ε_4 ranging from 0.93 to 0.99 using 91 soundings to represent a large range of atmospheric conditions. Previously, International Satellite Cloud Climatology

Project (Rossow and Schiffer, 1999) Advanced Very High Resolution Radiometer (AVHRR) data taken during 1986 and *Terra* MODIS data from April 2001 were processed using the same method described above to obtain channel 3, 4, and 5 emissivity maps (Chen et al. 2001, 2002). The resulting values of ε_3 from the data were within 1% of the original value for all of the cases with the largest errors occurring for some desert (0.73) areas. RMS errors as large as 3% were found for ε_4 with the greatest errors occurring over deserts. The values of T_3 from daytime AVHRR data were often saturated over desert areas due to high afternoon skin temperatures and highly reflective surfaces, the source of the large errors over deserts. The mean errors were all negligible. The theoretical calculations assumed an isotropic surface reflectance and no VZA dependence of ε.

The *Terra* MODIS data were analyzed by computing ε_3' for each clear nighttime pixel and averaging the results within every 10' latitude-longitude box for a given orbit. A mean value of ε_3' was computed for each region and used to derive ε_3, ε_4, ε_5, and ε_6, from the daytime data to obtain mean values and standard deviations for each region. The values of χ used in (8) were taken from the same models used by Trepte et al. (1999). Those models are generally applicable to visible or broadband solar channels. Averages were also computed for each IGBP surface type (Table 1) and used to fill in the results for regions with no data. These averages were only computed after filtering the regional results for unrealistic points that can arise due to poor representation of the actual temperature and humidity profiles by the ECMWF reanalysis, the presence of aerosols, or cloud contamination. The filters were developed from histograms of ε for each wavelength and IGBP type. Upper (1.0) and lower thresholds were set for each IGBP type and wavelength. *Terra* MODIS data fro the 4 months in 2002 and 2003 were processed in this manner.

4. RESULTS

Figures 1-4 show the distributions of ε_3 derived from July and October 2002 and January and April 2003, respectively. The lowest values, between 0.68 and 0.75, occur over deserts, particularly in the western Sahara, the Empty Quarter of the Arabian Peninsula, and the Takliman

Table 1. IGBP surface type.

1. evergreen needleleaf	2. evergreen broadleaf
3. deciduous needleleaf	4. deciduous broadleaf
5. mixed forests	6. closed shrublands
7. open shrubland	8. woody savannas
9. savannah	10. grasslands
11. permanent wetlands	12. croplands
13. urban	14. mosaic
15. snow/ice	16. desert
17. water	18. tundra
19. coastline = 10% to 90% water	

Table 2. Mean ε_3 for Northern Hemisphere.

IGBP	Jan 2003	Apr 2003	Jul 2002	Oct 2002
1	0.97	0.97	0.94	0.96
2	0.93	0.91	0.91	0.91
3	0.98	0.97	0.95	0.96
4	0.96	0.95	0.93	0.95
5	0.97	0.97	0.94	0.96
6	0.92	0.93	0.90	0.92
7	0.89	0.90	0.86	0.89
8	0.94	0.94	0.92	0.94
9	0.86	0.80	0.84	0.88
10	0.92	0.89	0.87	0.89
11	0.97	0.98	0.94	0.96
12	0.94	0.91	0.89	0.91
13	0.93	0.90	0.88	0.91
14	0.94	0.92	0.90	0.92
15	0.98	0.98	0.97	0.98
16	0.79	0.78	0.76	0.77
17	0.96	0.96	0.96	0.95
18	0.95	0.98	0.92	0.96
19	0.95	0.96	0.94	0.95

Table 3. Mean ε_3, ε_4, ε_5 and ε_6 for Northern Hemisphere

IGBP	3.7μm	11.0μm	12.0μm	8.5μm
1	0.96	0.99	0.99	0.92
2	0.91	0.98	0.96	0.95
3	0.96	0.99	0.99	0.92
4	0.95	0.99	0.99	0.94
5	0.96	0.99	0.99	0.94
6	0.92	0.98	0.98	0.91
7	0.89	0.97	0.98	0.90
8	0.94	0.99	0.98	0.93
9	0.88	0.97	0.96	0.94
10	0.89	0.97	0.97	0.92
11	0.96	0.99	0.99	0.90
12	0.91	0.97	0.98	0.94
13	0.91	0.97	0.97	0.93
14	0.92	0.98	0.98	0.94
15	0.98	0.99	0.99	0.91
16	0.77	0.93	0.95	0.82
17	0.95	0.99	0.98	0.94
18	0.96	0.99	0.99	0.90
19	0.95	0.99	0.98	0.92

Desert in northwestern China. In heavily vegetated areas, ε_3 is generally greater than 0.90 with smaller values during Desert in northwestern China. In heavily vegetated areas, the peak growing seasons. The emissivity decreases to values between 0.85 and 0.90 in semiarid regions and to less than 0.85 in drier regions. It is generally greater than 0.95 in wet, coniferous areas and areas with dormant deciduous trees and snow cover.

The mean values of ε_3 for each of the IGBP types in the Northern Hemisphere are summarized in Table 2. The greatest seasonal variations occur in the lightly vegetated savannahs, grasslands, shrublands, and deserts. The most barren deserts like the Sahara do not show much seasonal variation. Some of the IGBP types, like tundra and deciduous needleleaf forests, are not well sampled and are not reliable especially during winter months. The ocean and snow categories are probably cloud contaminated and are not used for CERES. Instead, theoretical models are used for water, snow, and ice surfaces. The water surface model is based on the emissivities developed by Masuda et al. (1988). The snow-ice theoretical emissivity model is based on adding-doubling radiative transfer calculations that assume the snow can be represented as an ice cloud with an optical depth of 100 consisting of a hexagonal ice column with an aspect ratio of 750 μm / 300 μm.

The mean October 2002 emissivities for each channel and IGBP type data in northern hemisphere are summarized in Table 3. The values for ε_4 and ε_5 are generally greater than their ε_3 counterparts, while the ε_6 values are between those for ε_3 and ε_4.

To assess the results, the TOA channel-3 brightness temperatures were calculated from *Terra* MODIS October 2002 data using the emissivity maps generated from the above method (method1) and the MODIS Land Surface Temperature Group (method2; see Ma et al., 2002), the observed values of T_4, and the ECMWF profiles. First, the skin temperature is derived from the observed T_4, the ECMWF profiles, and ε_4. Then, T_3 is computed using the skin temperature, ε_3, the ECMWF profiles, and the bidirectional reflectance models. Differences between the predicted and observed values of T_3 are summarized in Tables 4 and 5. Except for snow and urban surfaces, the mean daytime errors range from –0.5 to –1.8 K for method1 and from –4 to 0.5 K for method2. The standard deviations vary between 3.1 and 4.6 K for method1 and between 3.5 and 5.5 K for method2. At night, the standard deviations range between 2 and 4 K from both methods. Excluding IGBP types 2 and 13, method2 yields smaller biases than method1 at night with a range of –0.8 to 1.6 K compared with –2.2 to 0.3 K. The sparse sampling of type 13 and the great potential for cloud contamination for broadleaf evergreen forests may contribute to the larger biases for type 2 surfaces. The day-night bias differences may also be due to changes in the surface moisture (e.g., dew or ground fog; Minnis et al., 1998) between the two measurement times. Considering both the day and night differences, both methods produce comparable results.

Other factors, besides cloud contamination and soil moisture changes, that can produce errors in the emissivity retrievals include the use of the broadband bidirectional reflectance models for the 3.7-μm reflectance anisotropy, the possibility of a viewing zenith angle dependence of surface emissivity, errors in the temperature and humidity profiles, and inhomogeneities in the boxes used to average the values. Currently, no empirical or theoretical 3.7-μm anisotropic reflectance models are available for vegetated surfaces. Without such models, it will not be possible to minimize the impact of anisotropy on the retrieval. Simultaneous dual-angle views from different satellites could be used to estimate

Table 4. T_3 errors using ε_3 for October 2002, daytime

IGBP	ΔT (K) from method1		from method2	
	mean	std	mean	std
1	-0.83	4.04	0.12	4.30
2	-1.76	4.22	-3.99	5.23
3	-1.40	3.11	0.12	3.43
4	-1.23	4.24	-0.78	5.00
5	-0.99	3.87	0.46	4.36
6	-1.79	4.16	-2.98	5.50
7	-0.75	3.79	-2.67	4.42
8	-1.30	4.27	-2.33	5.40
9	-1.67	3.95	-4.59	4.96
10	-1.03	4.62	-2.45	5.29
11	-0.53	3.18	0.35	3.53
12	-1.20	3.89	-2.69	4.69
13	-2.06	3.80	-2.94	4.41
14	-1.37	4.22	-2.41	5.14
15	-3.29	6.26	-3.18	6.26
16	-0.75	3.09	-4.09	3.68
17	0.02	3.24	0.03	3.25
18	0.09	3.57	0.92	3.91
19	-0.01	5.13	0.26	5.39

Table 5. T_3 errors using ε_3 for October 2002, nighttime

IGBP	ΔT (K) from method1		from method2	
	mean	std	mean	std
1	-0.88	3.12	0.08	3.24
2	-3.52	4.33	-2.61	4.76
3	0.27	2.33	1.63	2.40
4	-1.49	3.54	-0.54	3.73
5	-1.16	3.31	-0.24	3.45
6	-1.74	3.74	-0.28	3.84
7	-0.61	3.13	0.27	3.17
8	-1.35	3.79	-0.27	4.06
9	-2.18	3.61	-0.80	3.91
10	-1.26	3.47	-0.26	3.54
11	0.24	2.97	1.44	3.08
12	-1.55	3.18	-0.56	3.36
13	-2.34	2.97	-1.27	3.02
14	-1.82	3.49	-0.87	3.70
15	-0.66	3.52	-0.43	3.54
16	-0.86	2.84	-0.08	2.83
17	-0.25	2.35	-0.24	2.35
18	0.71	3.06	1.87	3.07
19	-0.84	3.80	-0.28	3.89

the viewing zenith angle impact on the surface emissivity while higher spatial resolution data, like that used by Ma et al. (2002) can minimize the impact of spatial inhomogeneities. Given that the bias and standard deviations of the predicted T_3 are relatively small over deserts, it is likely that the atmospheric correction and surface moisture could have greatest impact on surface emissivity retrievals. Thus, properly accounting for those impacts is more challenging, especially in moist regions.

5. CONCLUDING REMARKS

Compared to more sophisticated multi-spectral approaches, the results of the simple method applied here yields reasonable daytime and nighttime predictions of T_3 for the MODIS data that were used in the determination of the emissivities. The current method explored is relatively simple and can be applied to most current operational satellite imager data. Although the results from this technique are currently being used to successfully predict clear-sky radiances for CERES cloud retrievals, there is still much room for improvement. Thus, the factors affecting the retrievals will be explored in the future to enhance the accuracy of the surface emissivity retrievals.

References

Chen, Y., S. Sun-Mack, P. Minnis, W. L. Smith, Jr., and D. F. Young, 2001: Surface emissivity derived for infrared remote sensing from satellites. *Proc. AMS 11th Conf. Satellite Meteorol. & Oceanog.*, Madison, WI, Oct. 15-18, 512-515.

Chen, Y., et al., 2002: Surface spectral emissivity derived from MODIS data. *Proc. SPIE Remote Sens. of Atmos.,* *Ocean, Environment, and Space*, Hangzhou, China, October 23-27, Vol. 4891, 361-369.

Kratz, D. P., 1995: The correlated *k*-distribution technique as applied to the AVHRR channels. *J. Quant. Spectrosc. Radiat. Transfer*, **53**, 501--517.

Ma, X.-L., Z. Wan, C. C. Moeller, W. P. Menzel, and L. E. Gumley, 2002: Simultaneous retrieval of atmospheric profiles, land-surface temperature, and surface emissivity from Moderate Resolution Imaging Spectroradiometer thermal infrared data: extension of a two-step physical algorithm. *Appl. Opt.*, **41**, 909-924.

Masuda, K., T. Takashima, and Y. Takayama, 1988: Emissivity of pure and sea waters for the model sea surface in the infrared window regions. *Remote Sens. Environ.*, **24**, 313-329.

Minnis, P., W. L. Smith, Jr., and D. F. Young, 1998: Surface emissivity derived from multispectral satellite data. Proc. *8th Annual ARM Sci. Team Mtg.*, Tuscon, AZ, March 23-27, 1998, 489-494.

Minnis, P., et al., 2003: CERES cloud property retrievals from imagers on TRMM, Terra, and Aqua. *SPIE 10th Intl. Symp Remote Sens., Conf. Remote Sens. Clouds and Atmos.*, Barcelona, Spain, Sept. 8-12, 37-48.

Rossow, W. B. and R. A. Schiffer, 1999: Advances in understanding clouds from ISCCP. *Bull Am. Meteor. Soc.*, **80**, 2261-2287.

Trepte, Q., et al., 1999: Scene identification for the CERES cloud analysis subsystem. *Proc. AMS 10th Conf. Atmos. Rad.*, Madison, WI, June 28 – July 2, 1999, 169-172.

Wielicki, B. A., et al., 1998, Clouds and the Earth's Radiant Energy System (CERES): Algorithm overview. *IEEE Trans. Geosci. Remote Sens.*, **36**, 1127-1141.
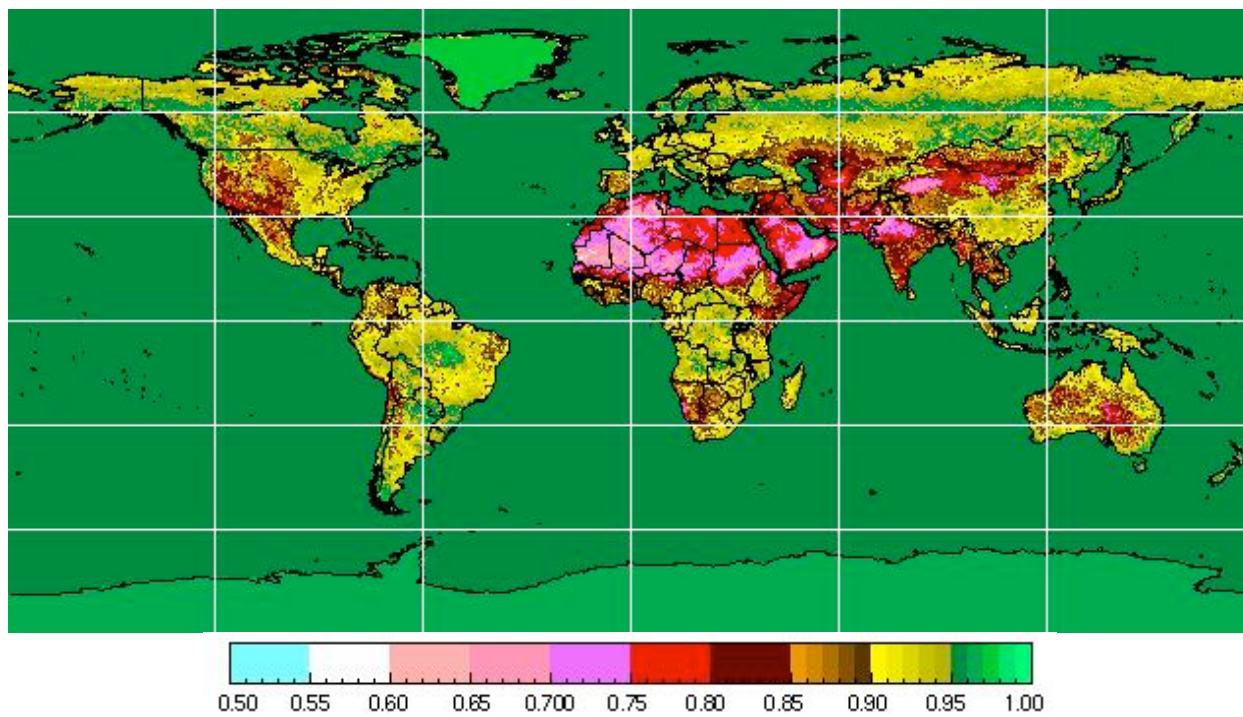
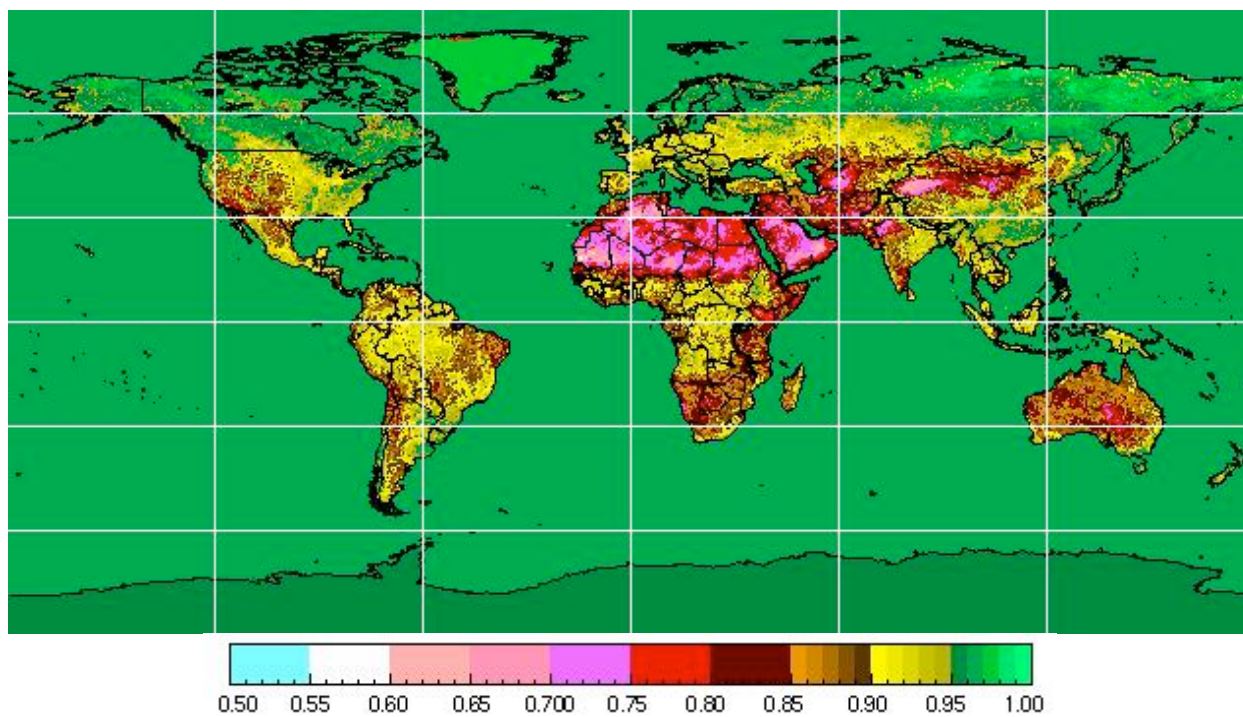Fig. 1. Mean 3.7-µm surface emissivities derived from Terra MODIS data, July 2002.

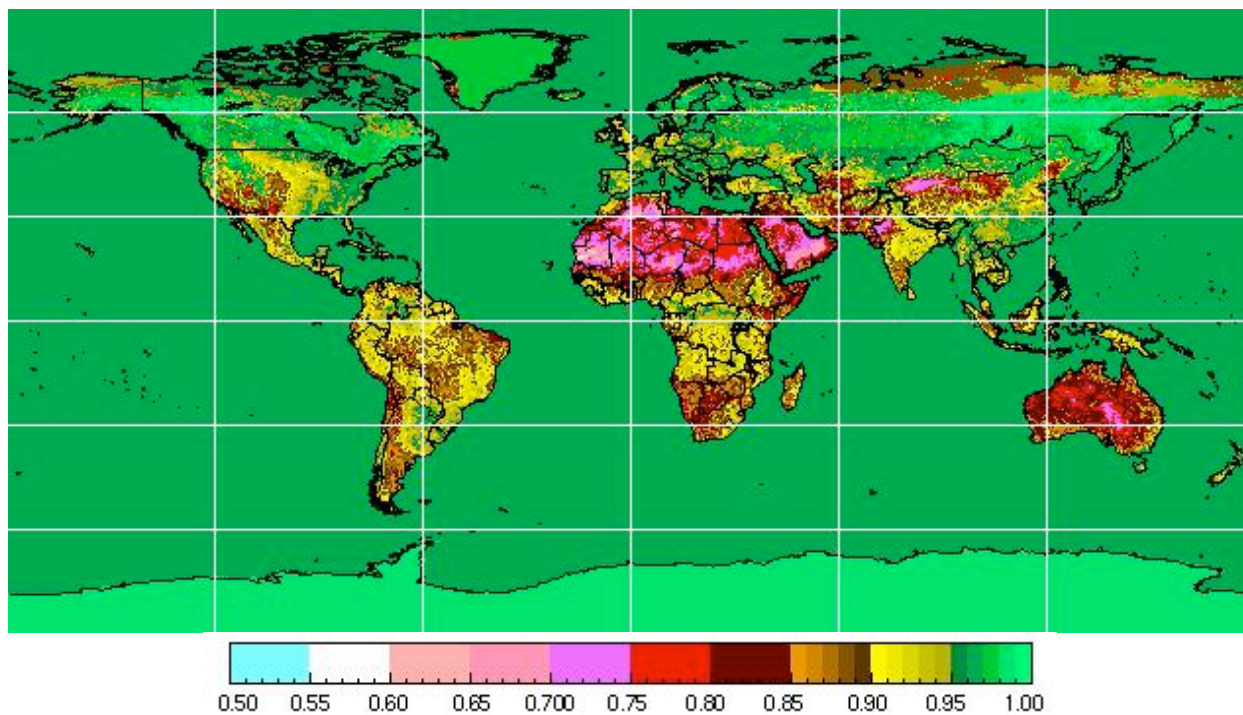Fig. 2. Mean 3.7-µm surface emissivities derived from Terra MODIS data, October 2002.

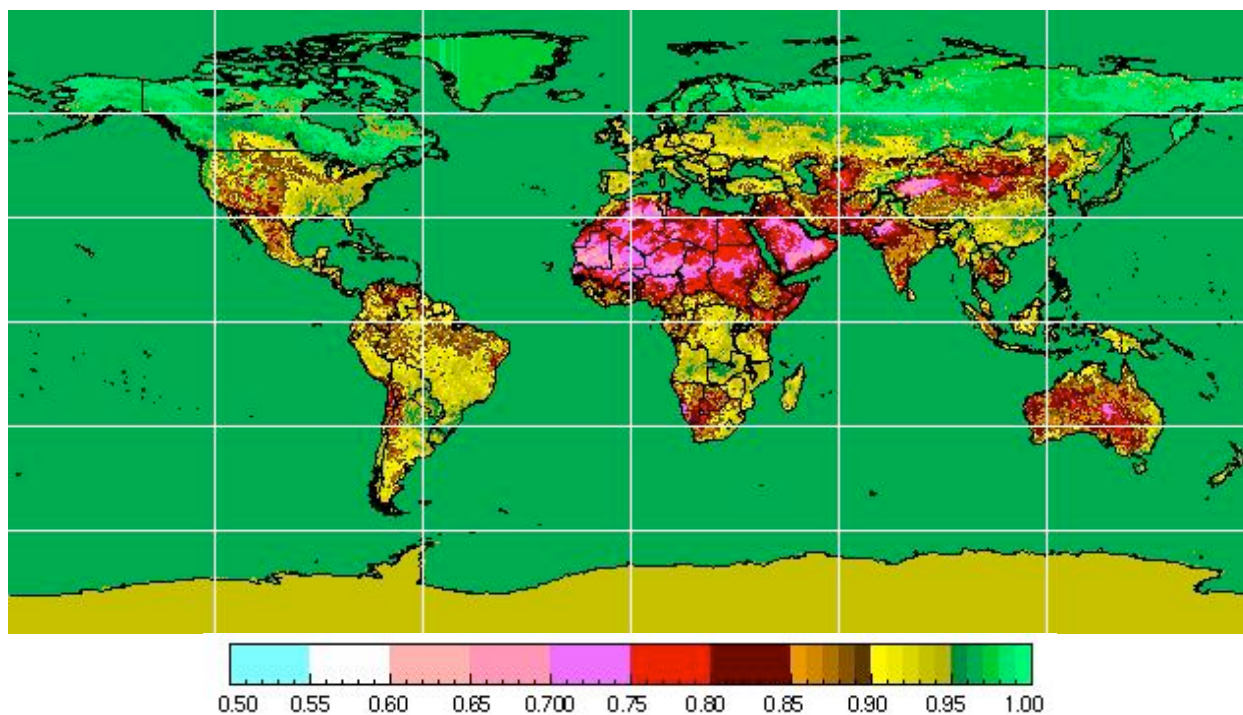Fig. 3. Mean 3.7-µm surface emissivities derived from Terra MODIS data, January 2003.

Fig. 4. Mean 3.7-µm surface emissivities derived from Terra MODIS data, April 2003.